



This is a repository copy of *Switched PI control based MRAS for sensorless control of PMSM drives using fuzzy-logic-controller.*

White Rose Research Online URL for this paper:
<https://eprints.whiterose.ac.uk/188908/>

Version: Published Version

Article:

Liu, Z.-H., Nie, J., Wei, H.-L. orcid.org/0000-0002-4704-7346 et al. (3 more authors) (2022) Switched PI control based MRAS for sensorless control of PMSM drives using fuzzy-logic-controller. *IEEE Open Journal of Power Electronics*, 3. pp. 368-381. ISSN 2644-1314

<https://doi.org/10.1109/ojpel.2022.3182053>

Reuse

This article is distributed under the terms of the Creative Commons Attribution-NonCommercial-NoDerivs (CC BY-NC-ND) licence. This licence only allows you to download this work and share it with others as long as you credit the authors, but you can't change the article in any way or use it commercially. More information and the full terms of the licence here: <https://creativecommons.org/licenses/>

Takedown

If you consider content in White Rose Research Online to be in breach of UK law, please notify us by emailing eprints@whiterose.ac.uk including the URL of the record and the reason for the withdrawal request.



eprints@whiterose.ac.uk
<https://eprints.whiterose.ac.uk/>

Switched PI Control Based MRAS for Sensorless Control of PMSM Drives Using Fuzzy-Logic-Controller

ZHAO-HUA LIU ¹, JIE NIE ¹, HUA-LIANG WEI ², LEI CHEN ¹,
XIAO-HUA LI ¹, AND MING-YANG LV ¹

¹School of Information and Electrical Engineering, Hunan University of Science and Technology, Xiangtan 411201, China
²Department of Automatic Control and Systems Engineering, University of Sheffield, S1 3JD Sheffield, U.K.

CORRESPONDING AUTHOR: ZHAO-HUA LIU (e-mail: zhaohualiu2009@hotmail.com)

This work was supported in part by the National Key Research and Development Project of China under Grant 2019YFE0105300, in part by the National Natural Science Foundation of China under Grants 61972443 and 62103143, in part by the Hunan Provincial Key Research and Development Project of China under Grant 2022WK2006, and in part by the Hunan Provincial Hu-Xiang Young Talents Project of China under Grant 2018RS3095.

ABSTRACT With the use of sensorless control strategy, mechanical position sensors can be removed from the gearbox, so as to decrease the maintenance costs and enhance the system robustness. In this paper, a switching PI control based model reference adaptive system (MRAS) observer using Fuzzy-Logic-Controller (FLC) is introduced for sensorless control of permanent magnet synchronous motor (PMSM) drives. The main work and innovation of this paper include: 1) A disturbance observer based voltage compensation method is proposed to solve the problems of voltage distortion in voltage source inverter (VSI) fed PMSM systems. 2) A double closed-loop FLC is designed for speed and current control. The response performance of speed regulation and the accuracy of the command voltage are improved, and the difficulty of manual adjustment of control parameters is avoided. 3) A sensorless control strategy of a switching PI control based MRAS observer is proposed for stator resistance tracking. By setting different thresholds, the proposed MRAS observer can choose the appropriate PI adaptive mechanism based on the amplitude of the current error variable, which can improve the accuracy of resistance estimation and improve the dynamic performance of sensorless control. 4) The experimental results are given to verify the availability of the proposed scheme.

INDEX TERMS Fuzzy logic control (FLC), model reference adaptive system (MRAS), proportion integration (PI), nonlinearity, PMSM, sensorless control, switching PI controller.

I. INTRODUCTION

Permanent-magnet synchronous motors (PMSM) have been broadly applied in electric vehicles, flywheel energy storage systems, and wind energy conversion systems in the recent years [1]–[3]. For speed and position regulation in the PMSM, there are two main control techniques: direct torque control (DTC) and field-oriented control (FOC). The DTC technique, on the other hand, has the disadvantages of low speed stability, torque ripple, and unreliability of parameter variation [4]. As a result of its efficiency for PMSM control and drive systems, the FOC algorithm is frequently employed in AC servo machines [5]. Unfortunately, the use of encoders, resolvers, Hall effect sensors or other mechanical position sensors increase

the maintenance costs and decrease the system robustness [6]–[8]. Therefore, the sensorless control methods have attracted extensive attention.

Position sensorless control methods can be classified into two types based on the speed range of PMSM operation: saliency-based high-frequency (HF) signal injection method and model-based back EMF method. Although the HF methods is suitable for sensorless PMSM control at low or zero speeds, it may cause torque ripple and extra loss, which has a negative impact on the system's dynamic performance and operation quality [9]. On the other hand, the EMF method has been extensively investigated because it does not require the injection of additional signals. It is widely recognized that

the model-based method is appropriate for PMSM to work at medium and high speeds [10]. In many sensorless control systems using back EMF, the steady-state module of PMSM is often utilized as a reference; consequently, robustness may be difficult to achieve if there is a parameter mismatch or load sudden change during the working operation under the low speed range [11], [12]. Due to the stator resistance of PMSM varies with temperature, robustness and precise multi-parameter identification is necessary for low speed sensorless driver [13], [14]. Therefore, some multi-parameter identification technologies such as extended Kalman filter (EKF) scheme [15], [16], recursive least squares (RLS) scheme [17], [18], and model reference adaptive system (MRAS) scheme [19] have been proposed. In [16], the EKF scheme gave appropriate experimental result in parameter identification. Nevertheless, the control algorithm has some limitations such as complex algorithmic structure, requirement of proper initialization. The RLS scheme for estimating electrical parameters proposed in [17] and [18] has a fast convergence speed. Unfortunately, due to the algorithm involves a large number of differential equations, the performance of micro-processor decreases and the system response is slow.

Among the parameter identification methods mentioned above, MRAS scheme has the advantages of simplicity, good stability and small amount of calculation, which has been testified to be one of the best methods introduced in the literature [20]. Usually, a single PI controller with simple structure is adopted in the MRAS scheme to calculate the position or rotor speed of PMSM. However, voltage-source inverter (VSI) nonlinearity and the change of PMSM parameter become more important at low speed operation. All this can make the single PI controller unable to maintain the robustness of the control system. Therefore, a variety of solutions with more advanced algorithms are proposed, which provide alternatives to the adaptation mechanism for MRAS scheme. In [21], a fuzzy logic controller (FLC) was employed in MRAS for speed regulation so that system are more robust than a PI controller to parameter uncertainties and sensor noises. In [22], A two-dimensional FLC based MRAS method was introduced for PMSM sensorless control. However, the method may be more complicated and computationally expensive when it is adopted in the MRAS scheme to replace the conventional PI adaptation mechanism. In [23], an artificial neural network (ANN) method had been utilized in MRAS scheme for stator resistance estimation and good experimental results have been obtained. In this paper, the switching PI control is designed based on the MRAS observer for realizing stator resistance tracking, which can improve the robustness of sensorless control for PMSM.

In addition, as a high-performance control method of PMSM, the core of FOC technology is to regulate the excitation current i_d and torque current i_q , respectively. The currents i_d and i_q can be calculated from the three phase currents i_a , i_b , and i_c (which can be obtained by current sensors) by clark/park transformation [24]. Traditionally, the proportional-integral (PI) controller is usually utilized in

many industrial applications because of their simple implementation. The fixed-gain PI controller is mainly affected by the parameter variation and external disturbance such as step changes of reference speed and load sudden change. Accordingly, PI controller cannot guarantee a reasonable dynamic and steady-state performance during the whole working operation range. For overcoming the disadvantage, some improved controllers are proposed [25]–[29]. In [25], Yasser *et al.* employed d -axis sliding-mode control method to displace the conventional d -axis PI current controller in torque-control technology and achieved good performance. In the FLC scheme, the control parameters can be adjusted properly by fuzzy rules, which can be used to build a logical model of the mankind behavior [26]. In conclusion, the FLC has clear edges over the conventional PI controller: 1) it is more simple and has less intensive mathematical design requirements; 2) it is more stable than the traditional PI controller; 3) it has the ability to deal with nonlinear function with arbitrary complexity [27]. The expert system and fuzzy logic have been employed for servo system to enhance control performance. In [28], a self-tuning PI control method using ANN was introduced to train the regulator to meet the design requirements under various working conditions. Besides, a recurrent fuzzy neural cerebellar model articulation network was also introduced in [29]. Although these intelligent methods seem to be powerful in some specific situations, the large amount of training is inevitable.

Moreover, a VSI is employed to supply power to the PMSM, and the voltages required by MRAS observer are obtained from the PI controller in the FOC drive of the PMSM. The voltage used for MRAS observer is often derived from the output signal of current loop, while the terminal voltage of PMSM is obtained from VSI, which is hard to measure [30]. It should be noted there is usually an error caused by the VSI nonlinearity between the output signals of the current loop and the output voltages of VSI. Therefore, the VSI nonlinearity should be compensated properly for improving the control performance of PMSM [31]. Generally, the VSI turbulence voltage is estimated by utilizing the related parameters of switching devices, and then the reference is compensated [32]. In this paper, the VSI nonlinearity caused by VSI is calculated by the disturbance observer, which is compensated properly.

In this manuscript, a FLC is introduced for speed and current controller. The parameters (i.e., K_p and K_i) can be adjusted by utilizing fuzzy control rules. The presented scheme can enhance the control performance of rotor speed and the precision of command voltage. Furthermore, the VSI nonlinearity caused by VSI is calculated by the disturbance observer, which is fed back to the d/q current controller. In the end, the switching PI control is designed based on the MRAS observer for realizing stator resistance tracking, which can enhance the robustness and accuracy of sensorless control. The main work of this manuscript is concluded as follows:

- 1) A disturbance observer based voltage compensation method is proposed to solve the problems of voltage distortion in VSI fed PMSM systems. The VSI nonlinearity

in the rotor rotating coordinate system are investigated. The disturbance voltage caused by the dead time and non-ideal switching characteristics of the IGBT is then compensated to the d - q axis current loop in a feedforward manner, reducing the error between the command voltage of the PI controller and the actual output voltage of VSI.

- 2) A FLC is designed for speed and current regulator control to ensure robust response. Since the speed error (E) and error change speed (EC) of current regulator are smaller than that of speed controller, five membership functions (MF) are applied to reduce the amount of calculation. In addition, the membership functions are designed to be more dense at the origin for improving the steady-state control performance. In addition, an improved fuzzy rule is designed to make the output adjustment of FLC more appropriate.
- 3) To ensure an accurate reference tracking, a switching PI system is proposed to replace the traditional PI adaptive mechanism for resistance tracking in the MRAS observer. The principle of this approach is simple and easy to implement. Under this scheme, the MRAS observer can choose proper PI controller and further determine whether the integral coefficients K_i (see Fig. 7) is needed to avoid overshoot and achieve robust response against different uncertainties such as parameter variation.

We organize this paper in the following parts. In Section II, the relevant functions of PMSM are analyzed and presented by considering the VSI nonlinearities. In Section III, a FLC scheme for speed and current regulators is proposed. In Section IV, an MRAS with a switching PI scheme is proposed. The relevant Simulink results are exhibited in Section V to show the robustness and stability of the proposed method. Finally, brief conclusions are given in Section VI.

II. MODELING OF PMSM CONSIDERING VSI NONLINEARITY

As we know, the 3-phase surface-mounted PMSM has the characteristics of $L_d=L_q=L_\alpha=L_\beta=L$ and the stator voltages for PMSM under d/q axis can be depicted as:

$$\begin{cases} u_d = R_s i_d + L \frac{d}{dt} i_d - \omega_e L i_q \\ u_q = R_s i_q + L \frac{d}{dt} i_q + \omega_e L i_d + \omega_e \psi_m \end{cases} \quad (1)$$

$$\begin{cases} \psi_q = L i_q \\ \psi_d = L i_d + \psi_m \end{cases} \quad (2)$$

where subscript d and q represents the d - q axis, u_d and u_q are stator voltage components, i_d and i_q are stator current components, L_d and L_q are the stator inductances, ψ_d and ψ_q are rotor flux components, R_s is the stator resistance, ω_e is the electrical angular velocity, ψ_m is the PM flux.

For the surface-mounted PMSM, the torque under the control strategy $i_d=0$ could be reported as:

$$T_e = 1.5P \psi_m i_q \quad (3)$$

TABLE 1 Relevant Parameters of the VSI

| | | | |
|--------------------|--------------------|-----------------------|--------------------|
| DC bus voltage | 560 [V] | Switch period | 86.9 [μ s] |
| Dead-time | 4 [μ s] | Switch device | IGBT |
| Turn-on time | 0.8-2.0 [μ s] | Turn-off time | 2.0-2.9 [μ s] |
| Saturation voltage | 1.8-2.7 [V] | Diode forward voltage | 2.2-2.3 [V] |

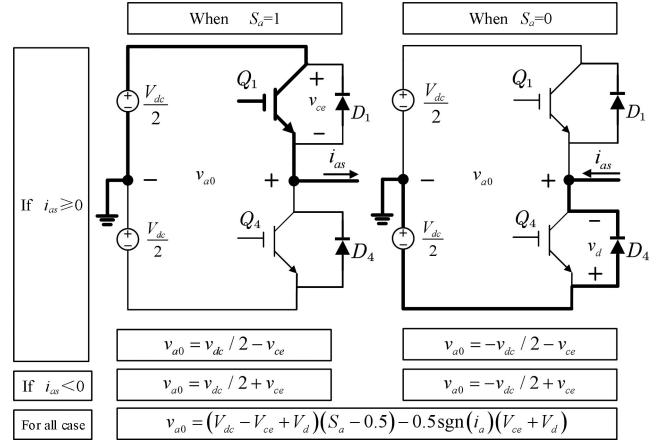


FIGURE 1. The block diagram of A phase arm of VSI.

$$J \frac{d\omega_m}{dt} = T_e - T_l - B\omega_m - T_f \quad (4)$$

where P is the number of pole pairs, J and B are inertia and viscous friction, respectively, ω_m is the mechanical angular velocity, and T_e and T_l are electrical and load torque.

Because the switch time of the industrial device is finite, it is necessary to consider dead time of pulse width modulation (PWM) gate signal for preventing two switch devices on the same arm of inverter from conducting at the same time. Table 1 gives the specifications of VSI. It is not hard to state the dead-time effect of A phase arm. Fig. 1 exhibits the structure diagram of A phase arm of the PWM inverter, where the insulated gate bipolar transistors are employed as switch equipment. In the course of T_d , both the switch devices Q_1/Q_4 in the same arm are closed, so the flow direction of the phase current i_a determines the output voltage. When the flow direction of the i_a is positive, the i_a flows through the bottom diode D_4 in the course of dead-time, and vice versa.

According to Fig. 2, considering the dead-time compensation voltage (DTCV), equation (1) update as:

$$\begin{cases} u_d^* + u_{d.com} = R_s i_d + L \frac{d}{dt} i_d - \omega_e L i_q + u_{d.dead} \\ u_q^* + u_{q.com} = R_s i_q + L \frac{d}{dt} i_q + \omega_e L i_d + \omega_e \psi_m + u_{q.dead} \end{cases} \quad (5)$$

where $u_{d.com}$ and $u_{q.com}$ are d - and q -axis voltage compensation of VSI nonlinearity, respectively, $u_{d.dead}$ and $u_{q.dead}$ are d - and q -axis disturbance voltage caused by VSI nonlinearity, respectively. In addition, the turbulence voltage in the rotating coordinate system under the control strategy $i_d=0$ can be

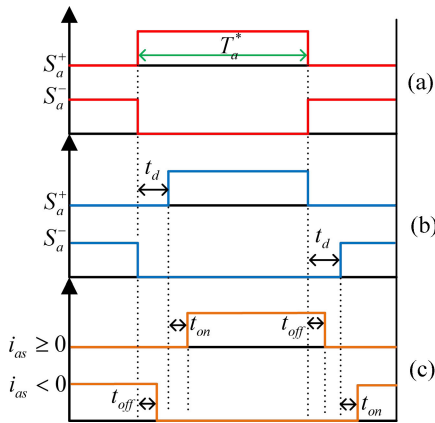


FIGURE 2. The gate trigger pulse of A-phase bridge arm.

represented as follows:

$$\begin{bmatrix} V_{q,dead} \\ V_{d,dead} \end{bmatrix} = V_{dead} \cdot \mathbf{K}^r(\theta_r) \begin{bmatrix} \text{sgn}(i_{qs} \cos \theta_r) \\ \text{sgn}(i_{qs} \cos(\theta_r - \frac{2\pi}{3})) \\ \text{sgn}(i_{qs} \cos(\theta_r + \frac{2\pi}{3})) \end{bmatrix} \quad (6)$$

$$V_{dead} = \frac{T_{dead} + T_{on} - T_{off}}{T_s} \cdot (V_{dc} - V_{sat} + V_d) + \frac{V_{sat} + V_d}{2} \quad (7)$$

where V_{dead} is the disturbance voltage, T_{on} and T_{off} are turn-on/off delay time, respectively, T_d is dead time, V_{sat} is saturation voltage drop of the active switch, V_d is diode forward voltage. $\mathbf{K}^r(\theta_r)$ is the rotation factor and can be depicted as:

$$\mathbf{K}^r(\theta_r) = \frac{2}{3} \begin{bmatrix} \cos(\theta_r) & \cos(\theta_r - \frac{2\pi}{3}) & \cos(\theta_r + \frac{2\pi}{3}) \\ \sin(\theta_r) & \sin(\theta_r - \frac{2\pi}{3}) & \sin(\theta_r + \frac{2\pi}{3}) \end{bmatrix} \quad (8)$$

III. THE PROPOSED FUZZY LOGIC CONTROLLER FOR SPEED AND CURRENT LOOP

The design of the PI controller depends on exact machine model. However, it is difficult for PMSM to obtain accurate d - q axis reactance parameters, this makes it difficult for PI controller design. Moreover, the single PI controllers are susceptible to parameter variation, hence FLC is employed in speed and current dual close-loop controller to replace the PI controller. The detailed chart of the FLC is illustrated in Fig. 3, where S_{ref} , S_{fb} and C_{ref} stand for reference rotor speed, rotor speed feedback and reference current, respectively. It includes a PI controller and a fuzzy inference system. The design of FLC contains the following parts: 1) fuzzification, 2) MF of fuzzy inference system, 3) fuzzy rules, and 4) the input scaling factors K_e and K_{de} , and output scaling factors K_1 and K_2 (which are defined in Fig. 3).

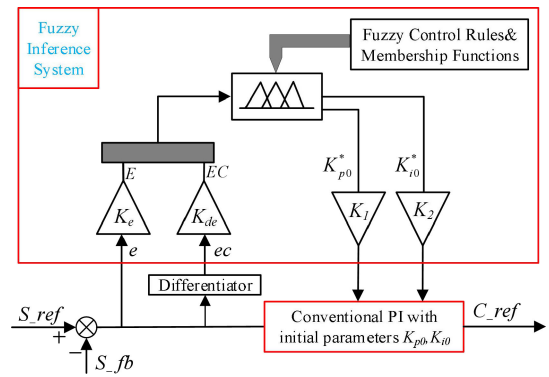


FIGURE 3. The diagram of a FLC for speed and current controllers.

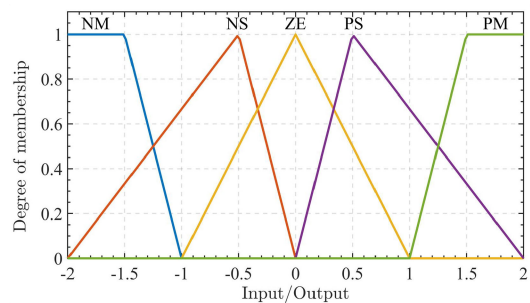


FIGURE 4. The MF for input and output of current controller.

A. FUZZIFICATION

Fuzzy set can be expressed as MF μ_H that associates with each element x of the universe of discourse X , a number $\mu_H(x)$ in the interval $[0, 1]$. The fuzzifier maps a clear input $x \in X$ to a fuzzified value $H \in U(\text{Universe})$.

- 1) *Singlet fuzzification*: fuzzy set H with support x_i , when $x = x_i$, $\mu_H(x_i) = 1$, while $\mu_H(x_i) = 0$, for $x \neq x_i$.
- 2) *Non-singlet fuzzification*: when $x = x_i$, $\mu_H(x_i) = 1$, and it decreases from 1 to 0 when the distance away from $x = x_i$.

Besides the experimental trial-and-error method, the initial parameters of PI controller can also be estimated by simulations (see e.g., [33]). In practical application, the results can be directly employed to the control system design if the PI controller is utilized, however, they are only used a reference for setting up the initial values for the FLC.

B. DESIGN OF MF

The MF of Mandani FLC for input maps the normalized E and EC to the membership degree from 0 to 1. The scaling factors K_e and K_c are used for transforming the input into the fuzzy variables E and EC , respectively. The transformation can be described as:

$$\begin{cases} E = eK_e \\ EC = ecK_c \end{cases} \quad (9)$$

where e is error, and ec is error change rate.

A total of seven linguistic terms are considered for fuzzy partition to be used for the speed controller design, namely,

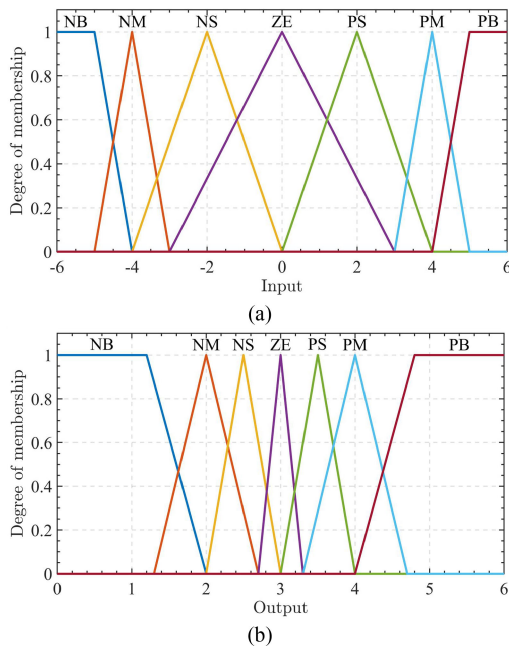


FIGURE 5. The MF for speed controller. (a) Input (E and EC). (b) Output (ΔK_p , ΔK_i).

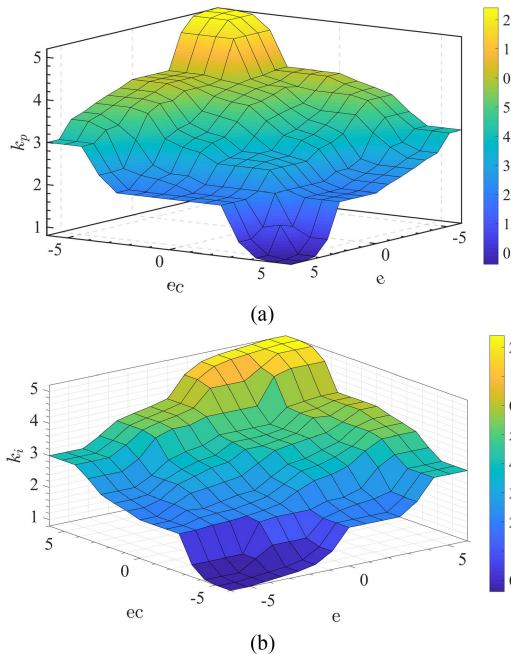


FIGURE 6. The output surface of speed controller. (a) K_p . (b) K_i .

1) Positive Large (PL), 2) Positive Medium (PM), 3) Positive Small (PS), 4) Zero (ZE), 5) Negative Small (NS), 6) Negative Medium (NM), and 7) Negative Large (NL). Because E and EC are smaller than that of speed controller, 5 variables are considered in the current controller to reduce the calculation cost. Note that in the current controller, 5 linguistic variables are selected in the interval $[-2, 2]$ as shown in Fig. 4. In terms of speed controller, the domains of E and EC are $[-6,$

$6]$, while the domain of U is $[0, 6]$. Because E and EC are larger than that of the current error, 7 variables (rather than 5) are selected as shown in Fig. 5. At both ends of the universe of discourse, the shape of fuzzy sets is trapezoidal, while the other intermediate fuzzy sets are triangular and overlap each other. The MF of the input characterized by FLC becomes insensitive when the input value is very small. As for the MF of the output, when E and EC remain small, the initial adjustment values (k_{p0}^* , k_{i0}^*) barely change. Unlike the MF proposed in [34], the MF proposed in this paper focus on the dynamic and steady-state effectiveness of the control system.

C. DESIGN OF FUZZY RULES

In this paper, max-min composition reasoning method of Mamdani is employed. Depending on fundamental knowledge and expert experience, fuzzy rules, as the bond between input and output, play a crucial rule for achieving satisfactory control performance. Fuzzy control rule base is a set of IF-THEN rules, which can be expressed as:

$$R^l : \text{IF } x_1 \text{ is } F_1^l \text{ and } x_2 \text{ is } F_2^l \text{ and } \dots \text{ and } x_j \text{ is } F_j^l \\ \text{THEN } y_1 \text{ is } G_1^l \text{ and } y_2 \text{ is } G_2^l \text{ and } \dots \text{ and } y_k \text{ is } G_k^l$$

where $x_1 \in X_1, \dots, x_j \in X_j$ are the input linguistic variables, and $y_1 \in Y_1, \dots, y_k \in Y_k$ are the output linguistic variables. F_n^l is the input fuzzy labels, G_m^l is the output fuzzy labels, the range of n is $1, \dots, j (j \in N)$, the range of m is $1, \dots, k (k \in N)$. R^l is the fuzzy link between fuzzy input set X to fuzzy output set Y .

The design of fuzzy rules for PMSM is depended on the following criteria [35]:

- 1) When E is large, smaller ΔK_i and larger ΔK_p should be chosen to decrease overshoot and accelerate the response of the system.
- 2) When E is medium, small ΔK_i and moderate ΔK_p should be removed; When EC is medium, increase ΔK_i and ΔK_p to improve the steady-state effectiveness of the control system.
- 3) When E and EC are small, large ΔK_i and ΔK_p should be adopted to decrease error and improve the response speed of control system.

In the current controller, the MF with higher density near the origin can improve the steady-state accuracy. The output surface of the fuzzy reasoning system is shown in Fig. 6. According to the above analysis, the control rules for the speed controller and current controller are exhibited in Tables 2 and 3, respectively.

D. DESIGN OF INPUT/OUTPUT SCALING FACTORS

K_e and K_{de} , as scaling factors, are utilized to map E and EC to the fuzzy region between -1 and 1 . They are similar to the gain coefficients of conventional PI controller and affect the stability, oscillations, and damping of the system. Therefore, K_e and K_{de} need to be selected carefully. Considering that flux weakening operation is not required, K_e and K_{de} can be

TABLE 2 The Fuzzy Rules for K_p/K_i of Speed Controller

| $E \backslash EC$ | NB | NM | NS | ZE | PS | PM | PB |
|-------------------|-------|-------|-------|-------|-------|-------|-------|
| NB | PB/NB | PB/NB | PM/NB | PM/NM | PS/NM | PS/ZE | ZE/ZE |
| NM | PB/NB | PB/NB | PM/NM | PM/NM | PS/NS | ZE/ZE | ZE/ZE |
| NS | PN/NM | PM/NM | PM/NM | PS/NM | ZE/ZE | NS/PS | NS/PS |
| ZE | PM/NM | PS/NS | PS/NS | ZE/ZE | NS/PS | NM/PS | NM/PM |
| PS | PS/NS | PS/NS | ZE/ZE | NS/PS | NS/PS | NM/PM | NM/PM |
| PM | ZE/ZE | ZE/ZE | NS/PS | NM/PM | NM/PM | NM/PB | NB/PB |
| PB | ZE/ZE | NS/ZE | NS/PS | NM/PM | NM/PB | NB/PB | NB/PB |

TABLE 3 The Fuzzy Rules for K_p/K_i of Current Controller

| $E \backslash EC$ | NM | NS | ZE | PS | PM |
|-------------------|-------|-------|-------|-------|-------|
| NM | PM/NM | PM/NS | PS/NS | PS/ZE | ZE/ZE |
| NS | PM/NM | PM/NS | PS/NS | ZE/ZE | ZE/ZE |
| ZE | PS/NS | ZE/ZE | ZE/ZE | NS/PS | NM/PS |
| PS | ZE/ZE | ZE/ZE | NS/PS | NS/PS | NM/PM |
| PM | ZE/ZE | NS/PS | NS/PS | NS/PM | NM/PM |

described as:

$$K_e = 1/e_{max} = 1/n_N \quad (10)$$

$$K_{de} = 1/e_{cmax} \quad (11)$$

where e_{max} and e_{cmax} are the maximum values of E and EC respectively, which can be extracted by simulation. K_1 and K_2 are employed to adjust the initial correction values kp_0^* and ki_0^* to the final adjustment values kp^* and ki^* . Defuzzification of fuzzy variables is a key step in obtaining a real domain variable. The center of gravity defuzzification scheme is employed, which can be reported as:

$$Output = \frac{\sum_{k=1}^N i \mu_{c(k)}(i)}{\sum_{k=1}^N \mu_{c(k)}(i)} \quad (12)$$

where N is the amount of fuzzy rules, and $\mu_{c(k)}(i)$ stand for the output membership grade for the rule with the output subset.

IV. SWITCHING PI CONTROL BASED MRAS OBSERVER FOR SENSORLESS CONTROL

A. SWITCHING PI CONTROL FOR STATOR RESISTANCE TRACKING

The core mission of the control system is to estimate the rotor speed after the command changes or the stator resistance varies with temperature. Therefore, the MRAS model is used to calculate the speed, position, and resistance of PMSM in this paper. An adaptive PI regulator is commonly used in MRAS, as shown in (15)-(17). It can be known that the estimation of rotor speed is mainly affected by the PMSM parameters (i.e., stator resistance, inductance, and permanent flux). These parameters can change with load current and motor temperature. Therefore, this is why the MRAS observer with a fixed gains of adaptive mechanism can only work steadily and obtain higher accuracy in a certain speed range.

In this paper, the switching PI system is employed for improving the estimation accuracy of stator resistance and the

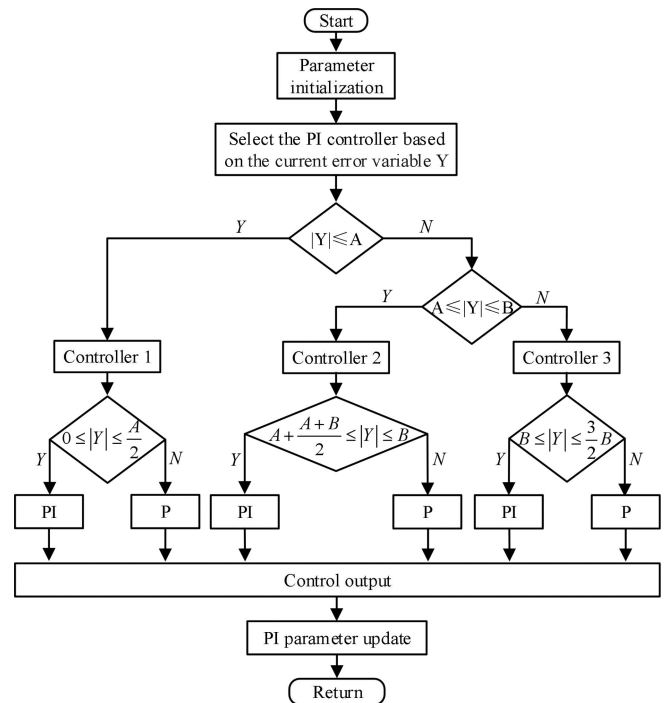


FIGURE 7. The flowchart of switching PI control based on MARS observer for resistance tracking.

robustness of speed estimation. Through different PI parameters, the sensitivity of the algorithm to the change of motor parameters is mitigated. In addition, the integral separation strategy is adopted: when the motor starts, the integral component would reduce the stability of the control system and increase the overshoot; in steady state, the integral composition can improve the regulation ability of the system and eliminate the error [36]. The flowchart of switching PI scheme is shown in Fig. 7. Let Y be the current error variable, which can be written as:

$$Y = [(i_q - \hat{i}_q) \hat{i}_q + (i_d - \hat{i}_d) \hat{i}_d] \quad (13)$$

The implementation of the switching PI scheme includes the following three steps:

- 1) The amplitude of current error variable Y is obtained through simulation.
- 2) Based on the amplitude of Y , two threshold values A and B are set. The amplitude is split further according to the designed threshold. When $A/2 \leq |Y| \leq B$, k_i is set to 0 to prevent overshoot; otherwise, k_i is increased to speed up the resistance tracking.
- 3) The design of other integral separation controllers is the same as those in 2).

B. STABILITY ANALYSIS OF THE MRAS OBSERVER

In [37], Popov's hyperstability criterion was used to derive the adaptive algorithm, which has been verified in theory. Substituting (2) into (1), the mathematical model of PMSM

current can be expressed as:

$$\frac{d}{dt} \begin{bmatrix} i_d \\ i_q \end{bmatrix} = \begin{bmatrix} -\frac{R_s}{L} & \omega_e \\ -\omega_e & -\frac{R_s}{L} \end{bmatrix} \begin{bmatrix} i_d \\ i_q \end{bmatrix} + \begin{bmatrix} \frac{u_d}{L} - \omega_e \frac{\psi_m}{L} \\ \frac{u_q}{L} \end{bmatrix} \quad (14)$$

In order to facilitate the analysis, the speed is constrained to the system matrix, and (14) is rewritten as:

$$\begin{bmatrix} \frac{d(i_d + \frac{\psi_m}{L})}{dt} \\ \frac{di_q}{dt} \end{bmatrix} = \begin{bmatrix} -\frac{R_s}{L} & \omega_e \\ -\omega_e & -\frac{R_s}{L} \end{bmatrix} \begin{bmatrix} i_d + \frac{\psi_m}{L} \\ i_q \end{bmatrix} + \begin{bmatrix} \frac{1}{L} & 0 \\ 0 & \frac{1}{L} \end{bmatrix} \begin{bmatrix} u_d + \frac{R_s \psi_m}{L} \\ u_q \end{bmatrix} \quad (15)$$

Let $i'_d = i_d + \frac{\psi_m}{L}$, $u'_d = u_d + \frac{R_s \psi_m}{L}$, $i'_q = i_q$, $u'_q = u_q$ and (15) can be rearrangement as

$$\begin{bmatrix} \frac{di'_d}{dt} \\ \frac{di'_q}{dt} \end{bmatrix} = \begin{bmatrix} -\frac{R_s}{L} & \omega_e \\ -\omega_e & -\frac{R_s}{L} \end{bmatrix} \begin{bmatrix} i'_d \\ i'_q \end{bmatrix} + \begin{bmatrix} \frac{1}{L} u'_d \\ \frac{1}{L} u'_q \end{bmatrix} \quad (16)$$

If (16) is expressed in the form of estimated value, the adjustable model is

$$\begin{bmatrix} \frac{d\hat{i}'_d}{dt} \\ \frac{d\hat{i}'_q}{dt} \end{bmatrix} = \begin{bmatrix} -\frac{R_s}{L} & \hat{\omega}_e \\ -\hat{\omega}_e & -\frac{R_s}{L} \end{bmatrix} \begin{bmatrix} \hat{i}'_d \\ \hat{i}'_q \end{bmatrix} + \begin{bmatrix} \frac{1}{L} u'_d \\ \frac{1}{L} u'_q \end{bmatrix} \quad (17)$$

where \hat{i}'_d and \hat{i}'_q are the estimated value of i'_d and i'_q , respectively. \hat{i}_d and \hat{i}_q are the estimated value of i_d and i_q , respectively. And $\hat{i}'_d = \hat{i}_d + \psi_m/L$, $\hat{i}'_q = \hat{i}_q$.

By subtracting (17) from (16), the state equation of current error can be obtained:

$$\frac{d}{dt} \begin{bmatrix} e_d \\ e_q \end{bmatrix} = \begin{bmatrix} -\frac{R_s}{L} & \omega_e \\ -\omega_e & -\frac{R_s}{L} \end{bmatrix} \begin{bmatrix} e_d \\ e_q \end{bmatrix} - (\hat{\omega}_e - \omega_e) \begin{bmatrix} 0 & 1 \\ -1 & 0 \end{bmatrix} \begin{bmatrix} \hat{i}'_d \\ \hat{i}'_q \end{bmatrix} \quad (18)$$

Abbreviate (18) as follows:

$$\frac{de}{dt} = \mathbf{A}e - (\omega_e - \hat{\omega}_e) \mathbf{J} \hat{i}'_s = \mathbf{A}e - \mathbf{w} \quad (19)$$

where $\mathbf{A} = \begin{bmatrix} -\frac{R_s}{L} & \omega_e \\ -\omega_e & -\frac{R_s}{L} \end{bmatrix}$, $\mathbf{J} = \begin{bmatrix} 0 & 1 \\ -1 & 0 \end{bmatrix}$, $\hat{i}'_s = \begin{bmatrix} \hat{i}'_d \\ \hat{i}'_q \end{bmatrix}$, $e = \begin{bmatrix} i'_d - \hat{i}'_d \\ i'_q - \hat{i}'_q \end{bmatrix}$.

The error system established according to (19) can be expressed in the form of state equation:

$$\begin{cases} \dot{e} = \mathbf{A}e - \mathbf{w} \\ v = \mathbf{C}e \end{cases} \quad (20)$$

where $\mathbf{w} = (\hat{\omega}_e - \omega_e) \mathbf{J} \hat{i}'_s$

Since (20) needs to satisfy two conditions of Popov stability:

- 1) Linear partial transfer function matrix. $\mathbf{G}(s) = \mathbf{D} + \mathbf{C}(s\mathbf{I} - \mathbf{A})^{-1}\mathbf{B}$ is strictly positive real matrix.
- 2) The nonlinear time-varying link satisfies Popov's integral inequality

In the following, the linear compensator \mathbf{C} and adaptive law in the error system diagram are designed to meet the stability conditions.

C. SELECTION OF LINEAR COMPENSATOR

According to the positive real lemma, the state equation of linear constant system is as follows:

$$\begin{cases} \dot{\mathbf{x}}(t) = \mathbf{A}\mathbf{x}(t) + \mathbf{B}\mathbf{u}(t) \\ \mathbf{y}(t) = \mathbf{C}\mathbf{x}(t) + \mathbf{D}\mathbf{u}(t) \end{cases} \quad (21)$$

where $\mathbf{x}(t)$ is the n-dimensional state vector; $\mathbf{y}(t)$ and $\mathbf{u}(t)$ are the m-dimensional output and input vectors of the controlled object respectively; \mathbf{A} , \mathbf{B} , \mathbf{C} and \mathbf{D} are constant matrices of corresponding dimensions.

The necessary and sufficient condition for $\mathbf{G}(s) = \mathbf{D} + \mathbf{C}(s\mathbf{I} - \mathbf{A})^{-1}\mathbf{B}$ to be strictly positive real matrix is the existence of a symmetric positive definite matrix. \mathbf{P} and real number matrices \mathbf{K} and \mathbf{L} , positive real number λ or symmetric positive definite matrix \mathbf{Q} , satisfy:

$$\begin{cases} \mathbf{P}\mathbf{A} + \mathbf{A}^T\mathbf{P} = -\mathbf{L}\mathbf{L}^T - 2\lambda\mathbf{P} = -\mathbf{Q} \\ \mathbf{B}^T\mathbf{P} + \mathbf{K}^T\mathbf{L}^T = \mathbf{C} \\ \mathbf{K}^T\mathbf{K} = \mathbf{D} + \mathbf{D}^T \end{cases} \quad (22)$$

For (20), since $\mathbf{B} = \mathbf{I}$, $\mathbf{D} = 0$, equation (22) can be rewritten as:

$$\begin{cases} \mathbf{P}\mathbf{A} + \mathbf{A}^T\mathbf{P} = -\mathbf{Q} \\ \mathbf{P} = \mathbf{C} \end{cases} \quad (23)$$

A necessary and sufficient condition for a real symmetric matrix to be positive definite is that the main subform of each order of the matrix is greater than zero. For SPMSM, since $L_d = L_q$, \mathbf{C} can be chosen as

$$\mathbf{C} = \begin{bmatrix} 1 & 0 \\ 0 & 1 \end{bmatrix} \quad (24)$$

According to (23), $\mathbf{P} = \mathbf{C}$ is a symmetric positive definite matrix. Substitute matrix \mathbf{A} and \mathbf{P} into (23):

$$\mathbf{Q} = -(\mathbf{P}\mathbf{A} + \mathbf{A}^T\mathbf{P}) = \begin{bmatrix} \frac{2R_s}{L} & 0 \\ 0 & \frac{2R_s}{L} \end{bmatrix} \quad (25)$$

Therefore, \mathbf{Q} is a symmetric positive definite matrix, and the motor parameters are independent of the rotor speed. From this, it can be proved that when the linear compensation matrix \mathbf{C} is (24), the transfer matrix $\mathbf{G}(s)$ of the linear forward channel is strictly positive and real.

D. PROOF THAT THE NONLINEAR TIME-VARYING ELEMENT SATISFIES POPOV STABILITY

The Popov integral inequality is as follows:

$$\eta(0, t_1) = \int_0^{t_1} \mathbf{v}^T \mathbf{w} dt \geq -\gamma_0^2 \quad (26)$$

where η is the integration of the inner product of the input and output, and γ_0 is a finite positive constant.

First, it is assumed that the mechanism of the MRAS velocity estimation system adaptation law is as follows:

$$\hat{\omega}_e = \int_0^t F_1(\mathbf{v}, t, \tau) d\tau + F_2(\mathbf{v}, t) + \hat{\omega}_e(0) \quad (27)$$

TABLE 4 Reference Parameters of the PMSM

| Parameters | Values |
|-----------------------------------|----------------|
| Nominal speed | 3000rpm |
| Nominal current I_N | 6.8A |
| Nominal voltage U_N | 380V |
| Nominal power | 4.0KW |
| DC bus voltage | 311V |
| d/q -axis inductance L_d/L_q | 15.86mH |
| Permanent magnet flux φ_f | 79mWb |
| Number of pole pairs p | 4 |
| Stator resistance Ω | 1.204 Ω |

TABLE 5 Parameters Employed in Switching PI for Resistance Tracking

| With integral | PI I | | PI II | | PI III | |
|------------------|-------|-------|-------|--------|--------|-------|
| Values | K_p | K_i | K_p | K_i | K_p | K_i |
| | 0.35 | 0.04 | 0.03 | 0.0015 | 0.02 | 0.001 |
| Without integral | P I | | P II | | P III | |
| Values | K_p | | K_p | | K_p | |
| | 0.35 | | 0.03 | | 0.02 | |
| Threshold | A | | | B | | |
| Values | 10 | | | 20 | | |

Substituting the values of system output v and nonlinear feedback w in (20) for v and w in (26):

$$\eta(0, t_1) = \int_0^{t_1} e^T C^T (\hat{\omega}_e - \omega_e) \mathbf{J} \hat{i}_s^T dt \quad (28)$$

Substituting (27) into (28), we can get:

$$\begin{aligned} \eta(0, t_1) &= \int_0^{t_1} e^T C^T \left[\int_0^{t_1} F_1(v, t, \tau) d\tau + \hat{\omega}_e(0) - \omega_e \right] \mathbf{J} \hat{i}_s^T dt \\ &+ \int_0^{t_1} e^T C^T F_2(v, t) \mathbf{J} \hat{i}_s^T dt \end{aligned} \quad (29)$$

Replace the two terms on the right side of the (29) with η_1 and η_2 , then η_1 and η_2 can be expressed as

$$\eta_1 = \int_0^{t_1} e^T C^T \mathbf{J} \hat{i}_s^T \left[\int_0^t F_1(v, t, \tau) d\tau + \hat{\omega}_e(0) - \omega_e \right] dt \quad (30)$$

$$\eta_2 = \int_0^{t_1} e^T C^T \mathbf{J} \hat{i}_s^T F_2(v, t) dt \quad (31)$$

Assume

$$\dot{f}(t) = e^T C^T \mathbf{J} \hat{i}_s^T \quad (32)$$

$$kf(t) = \int_0^t F_1(v, t, \tau) d\tau + \hat{\omega}_e(0) - \omega_e \quad (33)$$

where $k > 0$.

Substitute (32) and (33) into (30) to get:

$$\begin{aligned} \eta_1(0, t_1) &= \int_0^{t_1} \frac{df(t)}{dt} kf(t) dt \\ &= \frac{k}{2} [f^2(t_1) - f^2(0)] \geq -\frac{1}{2} kf^2(0) \geq -\gamma_0^2 \end{aligned} \quad (34)$$

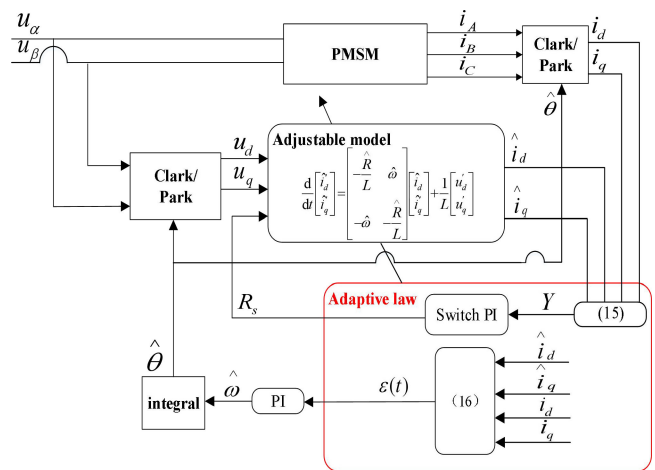


FIGURE 8. The improved MRAS observer based on switching PI scheme.

Taking the derivation of (33) and combining with (32):

$$F_1(v, t, \tau) = k_i e^T C^T \mathbf{J} \hat{i}_s^T \quad (35)$$

For (31), if the same takes:

$$F_2(v, t) = k_p e^T C^T \mathbf{J} \hat{i}_s^T \quad (36)$$

where $k_p > 0$, (31) must also be greater than $-\gamma_0^2$, η_1 and η_2 are greater than $-\gamma_0^2$ at the same time, so it is proved that the nonlinear time-varying link satisfies Popov stability.

Substitute e , C , J and \hat{i}_s^T obtained above into (35) and (36), and substitute the obtained results into (27) to obtain the estimated value of rotor speed. Equation (27) is usually written in the following form:

$$\hat{\omega}_e = \left(k_p + \frac{k_i}{s} \right) \left(i_d' \hat{i}_q - i_q' \hat{i}_d - \frac{\psi_m}{L} (i_q - \hat{i}_q) \right) \quad (37)$$

Define

$$\varepsilon(t) = i_d \hat{i}_q - i_q \hat{i}_d - \frac{\psi_m}{L} (i_q - \hat{i}_q) \quad (38)$$

Then the speed estimated by MRAS can be written as:

$$\hat{\omega}_e = \left(K_p + \frac{K_i}{s} \right) * \varepsilon(t) \quad (39)$$

Combining (13), the stator resistance estimated by MRAS observer can be written as:

$$\hat{R}_s = - \left(K_{pi} + \beta \frac{K_{ii}}{s} \right) Y \quad (40)$$

where β is the switching coefficient of the integral term. When $|Y| \leq A/2$, $\beta = 1$; otherwise $\beta = 0$. The identification equation of the electric angle is the integration of the identification equation of estimated speed:

$$\hat{\theta} = \int \hat{\omega}_e \quad (41)$$

Based on (38)–(41) and Fig. 7, the block diagram of the MRAS observer based on switching PI scheme is shown in Fig. 8. The whole block diagram of the MRAS observer for

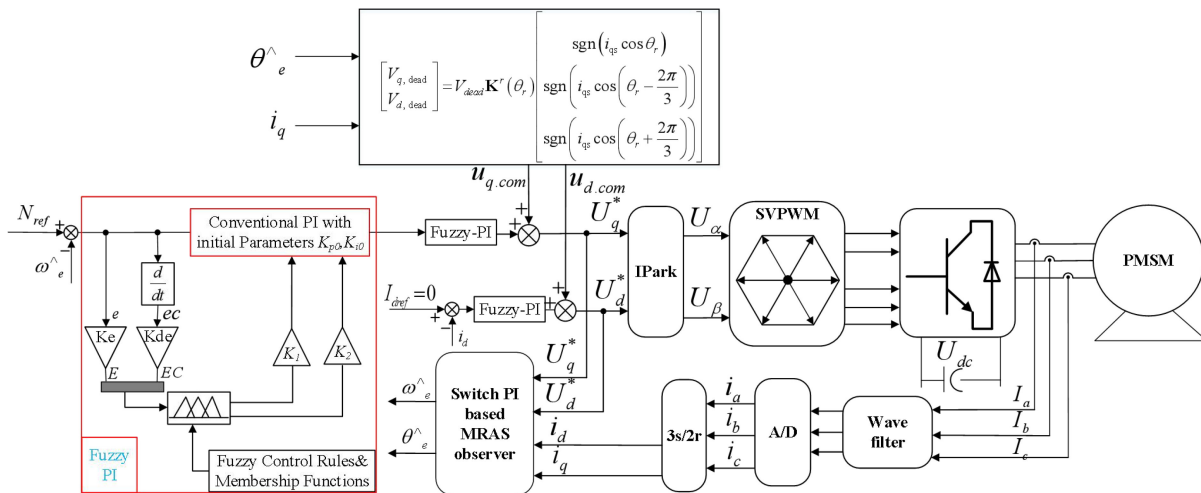


FIGURE 9. The diagram of the sensorless control system using the switching PI scheme based MRAS observer with FLC and VSI nonlinearity compensation strategy.

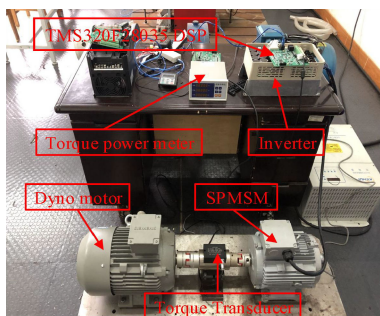


FIGURE 10. The used prototype PMSM.

estimating speed, position and resistance, fuzzy logic controller for speed and current loop, and the DTCV strategy, is exhibited in the Fig. 9.

V. EXPERIMENTAL WAVEFORMS AND ANALYSIS

A. CONFIGURATION OF THE PLATFORM

The DC bus is connected with the dc power source whose output is fixed to 311V, and the sampling frequency is set to 11.5 kHz. The utilized voltages and currents in the PMSM parameter estimation are measured from the output voltage of the current controllers as the terminal voltages of PMSM. The TMS320F28035 DSP is employed for parameter estimation of the prototype machine, and the identified parameters are used in the following simulation. All experiments are carried out on the same computer with intel(R) core(TM) i5-7500, four-core processors, RAM 16 GB and GPU of NVIDIA GeForce GTX 1050 Ti. The schematic diagrams of the hardware and software platforms are shown in Figs 10 and 11. The relevant parameters are exhibited in Table 4. The experimental results are exhibited to prove the robustness of the switching PI scheme based on MRAS observer for the sensorless control and stator resistance tracking of PMSM drives. The

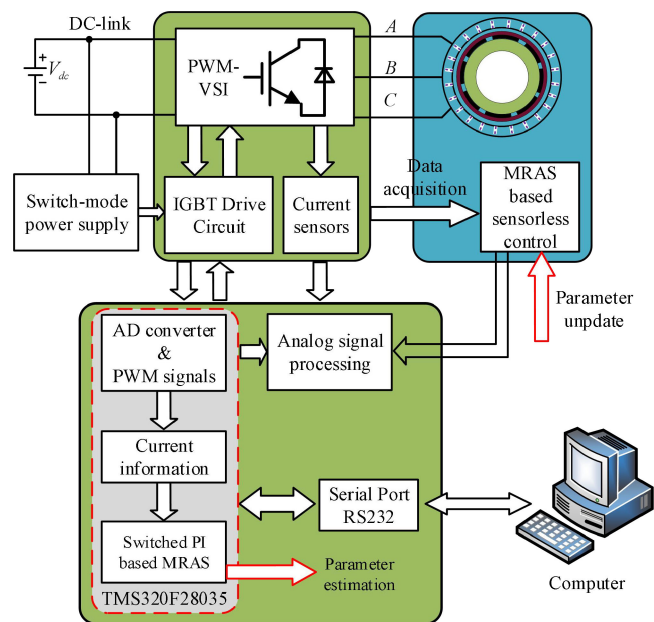


FIGURE 11. Schematic of hardware and software platform framework.

detailed gains used for the tuning of the adaptive mechanism of resistance are shown in Table 5. In all the tests, the double-closed-loop system of speed and current is employed. To testify the robustness of the system, the measured speed error during steady stage is studied by considering disturbance such as step change of speed command or stator resistance/ inductance/ permanent flux parameter variation.

B. EXPERIMENTAL RESULTS AND ANALYSIS

In order to show the superiority of the introduced switching PI scheme based on MRAS observer, the following five working conditions are introduced and investigated.

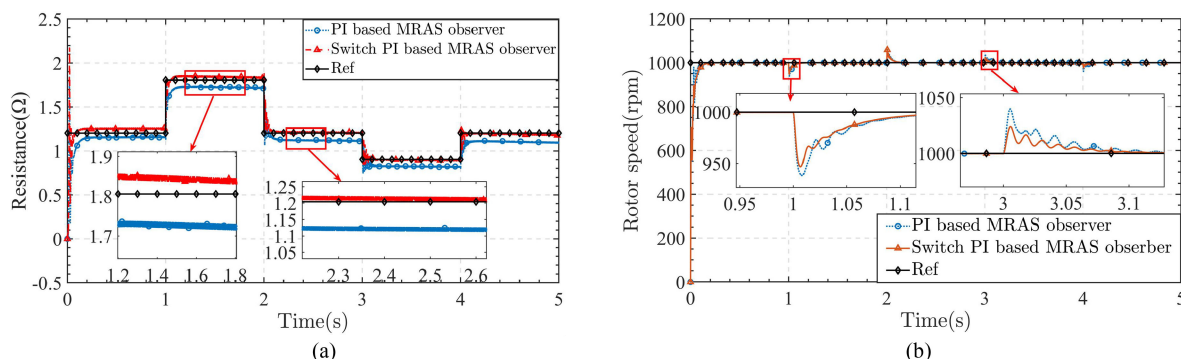


FIGURE 12. The comparison results for resistance variation ($1.204\Omega \rightarrow 1.806\Omega \rightarrow 1.204\Omega \rightarrow 0.903\Omega \rightarrow 1.204\Omega$). (a) Resistance tracking at 1000 rpm. (b) Rotor speed tracking under resistance variation.

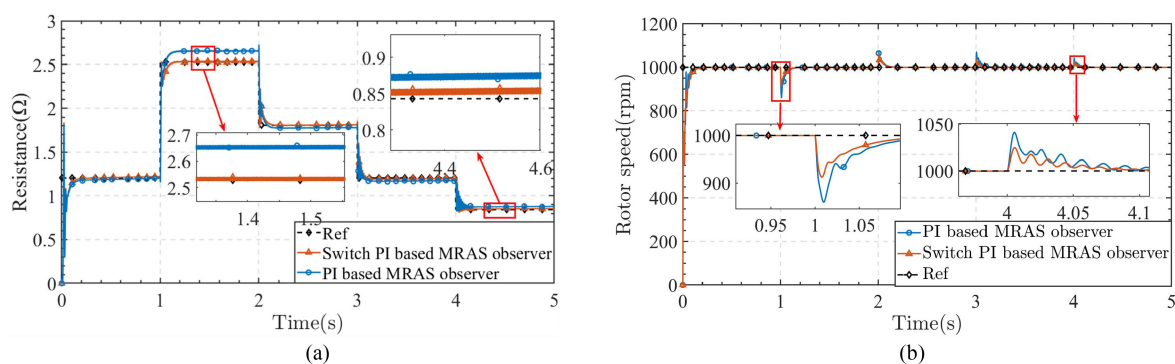


FIGURE 13. The comparison results for resistance variation ($1.204\Omega \rightarrow 2.528\Omega \rightarrow 1.806\Omega \rightarrow 1.0836\Omega \rightarrow 0.8428\Omega$). (a) Resistance tracking at 1000 rpm. (b) Rotor speed tracking under resistance variation.

1) *The Step Change of Stator Resistance:* In practice, the resistance of PMSM usually varies with the temperature. To reflect this fact and verify the robustness of control performance, in the experiments the big change of stator resistance is considered accordingly, and the reference speed is set as 1000 rpm. The experimental results based on two sets of resistance changes are shown in Figs. 12 and 13, where ‘Ref’ represents the reference value of stator resistance. In Fig. 12(a), the change process of resistance is as follows: 1.204Ω (initial value) $\rightarrow 1.806\Omega$ (1.5 times of the initial value) $\rightarrow 1.204\Omega \rightarrow 0.903\Omega$ (75% of the initial value) $\rightarrow 1.204\Omega$. It shows that the switching PI scheme has a higher accuracy for estimating the resistance than the conventional PI scheme. Fig. 12(b) shows the relevant estimated speed when the resistance changes. It shows that the steady-state and dynamic performance based on this method are better. When the resistance varies from 1.204Ω to 1.806Ω , the speed oscillates at the time of 1s and only takes 0.1 seconds to recover. Similarly, the speed changes at the time of 2s, 3s, and 4s due to the changes of the resistance. In Fig. 13(a), the change process of resistance is as below: 1.204Ω (initial value) $\rightarrow 2.528\Omega$ (2.1 times of the initial value) $\rightarrow 1.806\Omega$ (1.5 times of the initial value) $\rightarrow 1.0836\Omega$ (0.9 times

of the initial value) $\rightarrow 0.8428\Omega$ (0.7 times of the initial value). It shows that the steady-state error is less than 7.2%. The relevant estimated speed when the resistance changes is exhibited in Fig. 13(b). Therefore, the performance of the sensorless control for PMSM is effective in the proposed MRAS model based on the switching PI scheme via resistance tracking.

2) *The Step Change of Reference Speed:* In this experiment, the speed was set to be square wave signal but the stator resistance remains to be 1.204Ω . The step response (from 1000 rpm to 500 rpm) and the estimated values of the rotor speed are exhibited in Fig. 14(a). It shows that the estimated rotor speed based on the scheme of FLC can quickly track the command with a smaller steady-state error compared with the traditional PI controller. It also shows that there is no overshoot in the speed transition. The estimated rotor speed error is ± 0.1 rad/s. The error can be large only when the speed suddenly changes such as at 1s, 2s, 3s, and 4s. Fig. 14(b) shows that the zoomed estimation error of rotor position is at around $\pm 1^\circ$.

3) *The Effect of Stator Resistance Estimation:* The performance with the online estimation scheme for resistance is compared with that of without estimation scheme. The relevant results are exhibited in Fig. 15. Obviously,

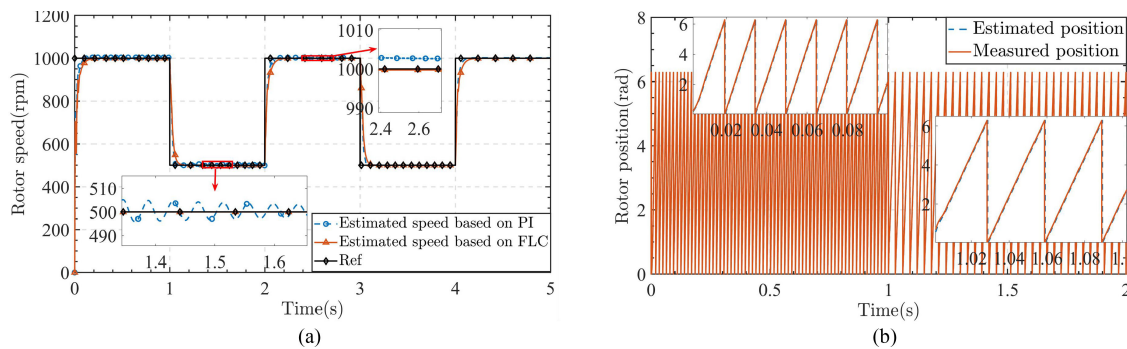


FIGURE 14. The experimental results for speed variation at 1.204Ω . (a) Rotor speed tracking varies from 1000 rpm to 500 rpm at 1.204Ω . (b) Zoomed rotor position estimation.

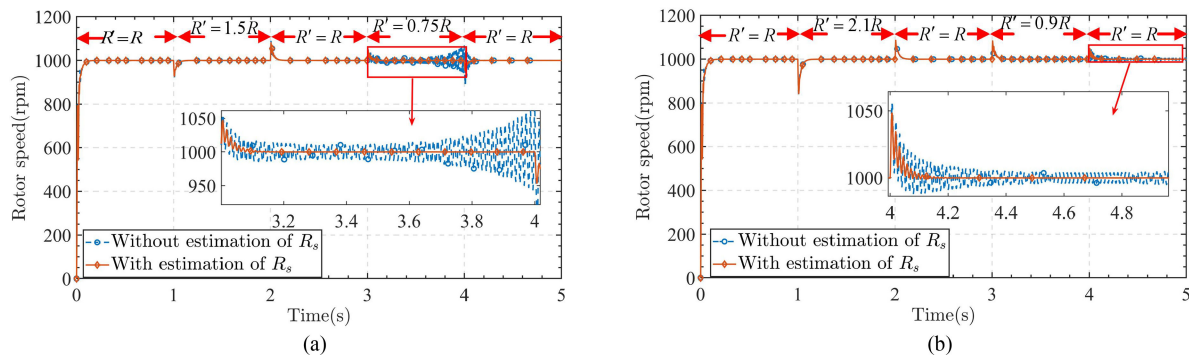


FIGURE 15. The speed tracking under resistance variation. (a) Comparison between online/no estimation of resistance ($1.204\Omega \rightarrow 1.806\Omega \rightarrow 1.204\Omega \rightarrow 0.903\Omega \rightarrow 1.204\Omega$). (b) Comparison between online/no estimation of resistance ($1.204\Omega \rightarrow 2.528\Omega \rightarrow 1.806\Omega \rightarrow 1.0836\Omega \rightarrow 0.8428\Omega$).

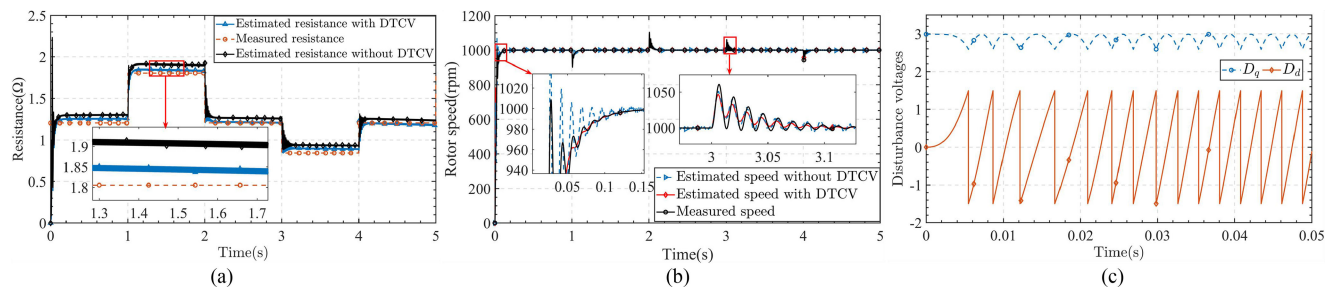


FIGURE 16. The speed tracking under resistance variation ($1.204\Omega \rightarrow 1.806\Omega \rightarrow 1.204\Omega \rightarrow 0.903\Omega \rightarrow 1.204\Omega$). (a) Comparison of speed estimation with and without DTCV strategy. (b) Comparison of stator resistance estimation with and without DTCV strategy. (c) The results of D_d/D_q under the $i_d = 0$ scheme and the reference rotor speed is 1000 rpm (Continuous line: q -axis turbulence voltage $V_{q,dead}$. Discontinuous line: d -axis turbulence voltage $V_{d,dead}$).

the dynamic performance and estimation accuracy of sensorless control are greatly improved if the stator resistance is online estimated.

- 4) *The Effect of DTCV Strategy:* The sensorless control performances, with/without DTCV are given in Fig. 16. It can be seen that the system with DTCV not only has higher efficiency but also will not appear overshoot and undershoot. The error of the estimated speed without DTCV is also larger than that with DTCV. The estimation of resistance is exhibited in Fig. 16(b). It shows that the resistance tracks more closely when DTCV is

considered. The experimental results of D_d and D_q are given in Fig. 16(c), under the $i_d = 0$ control method and the reference speed is 1000 rpm. It shows that the V_q^{com} is an alternating voltage and the V_d^{com} is the voltage with constant direction.

- 5) *The Step Change of permanent flux and inductance:* In addition to the sudden change of stator resistance, PMSM may have a demagnetization fault, resulting in the reduction of flux linkage. Therefore, the flux linkage step change needs to be taken into account. The inductance does not change during the flux linkage

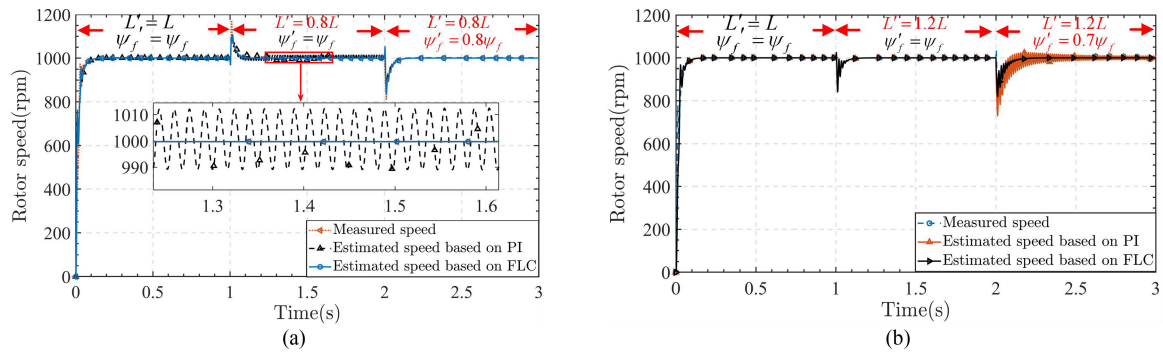


FIGURE 17. The comparative experimental results of speed estimation based on FLC and PI at 1.204Ω under inductance and permanent flux variation. (a) Under the working conditions of $L' = 0.8L$ and $\psi_f = 0.8\psi_f$. (b) Under the working conditions of $L' = 1.2L$ and $\psi_f = 0.7\psi_f$.

TABLE 6 The Detailed Comparison Under Different Control Strategy for Sensorless Control

| Speed and current controller | | PI controller | | | | Fuzzy logic controller | | | |
|--|-------------------|-----------------------------------|-----------|------------|-------|--------------------------------|-----------|------------|-------|
| Evaluation indicator | | Rise time | Overshoot | Undershoot | Error | Rise time | Overshoot | Undershoot | Error |
| Turbulence | Working condition | | | | | | | | |
| Resistance Remains Constant (1.204Ω) | 500rpm~1000rpm | 0.25s | 1.6% | 1.4% | 0.07% | 0.22s | 0 | 0 | 0.02% |
| Adaption machine for stator resistance tracing | | PI controller | | | | Switching PI controller | | | |
| The Change of Resistance (100%-150%-100%-75%-100%) | 1000rpm | 0.69s | 0.24% | 5.61% | 0.05% | 0.27s | 0.01% | 4.25% | 0.02% |
| The Change of Resistance (100%-210%-150%-90%-70%) | 1000rpm | 0.58s | 7.25% | 4.21% | 0.25% | 0.23s | 5.82% | 0.72% | 0.04% |
| The Change of Inductance and permanent flux ($L' = 0.8L$ and $\psi_f = 0.8\psi_f$) | 1000rpm | 0.32s | 0.25% | 1.08% | 0.42% | 0.25s | 0.12% | 0.03% | 0.05% |
| The Change of Inductance and permanent flux ($L' = 1.2L$ and $\psi_f = 0.7\psi_f$) | 1000rpm | 0.34s | 0.44% | 2.51% | 0.25% | 0.28s | 0% | 0.22% | 0.04% |
| VSI nonlinearity | | Without DTCV scheme | | | | With DTCV scheme | | | |
| The Change of Resistance (100%-150%-100%-75%-100%) | 1000rpm | 0.45s | 7.02% | 7.52% | 1.85% | 0.25s | 1.26% | 5.29% | 0.53% |
| Parameter identification | | Without resistance identification | | | | With resistance identification | | | |
| The Change of Resistance (100%-150%-100%-75%-100%) | 1000rpm | 0.26s | 8.42% | 7.26% | 2.02% | 0.22s | 8.01% | 7.21% | 0.03% |
| The Change of Resistance (100%-210%-150%-90%-70%) | 1000rpm | 0.34s | 9.03% | 16.7% | 1.24% | 0.23s | 8.65% | 15.9% | 0.02% |

mutation process. Fig. 17(a) shows the scenario where the inductance reduces to 80% of its initial value at $t = 1$ s, while the permanent magnet flux chain reduces to 80% its initial value at $t = 2$ s. The real value of inductance is 15.86mH. Due to the sudden change in inductance and flux linkage, the speed vibrates for a short period and then returns to the initial value. Furthermore, the speed estimation based on FLC scheme is more robust to parameter perturbation compared with PI. It can be seen from Fig. 17(b) that high-precision sensorless control can be achieved. Since the permanent flux changes to 70% of its initial value at $t = 2$ s, the speed drop is bigger than that in Fig. 17(a), but it can also return to the set value in a short time. Furthermore, PMSM has less speed estimation oscillation and better dynamic performance than PI controller under parameter perturbation because FLC can automatically adjust K_p and K_i parameters in real time. A detailed comparison exhibiting the superiority of the introduced scheme is shown in Table 6.

VI. CONCLUSION

In this manuscript, a switching PI system based on MRAS observer using dual close-loop FLC is introduced for sensorless control of PMSM field, which can help decrease the overshoot of stator resistance tracking and enhance the effectiveness of sensorless control. The working condition under the variable speed and multi-parameter perturbation is investigated. The sensorless control and resistance estimation considering DTCV strategy are also investigated. The following conclusions can be drawn from the experimental results:

- 1) The introduced dual close-loop FLC can quickly track the reference speed with a smaller steady-state error compared to traditional PI controller. In addition, a switching PI scheme based on MRAS observer is proposed. By setting different thresholds, the system can choose the appropriate PI adaptive mechanism based on the amplitude of the current error variable, improve the identification accuracy of stator resistance R_s , and further strengthen the robustness of PMSM sensorless control under parameter perturbation.

- 2) When the stator resistance changes from 2.1 times to 0.7 times, the MRAS observer can track closely and the error is less than 4.8%; there is little overshoot in the estimated resistance when the resistance changes suddenly. The control performance can be improved if the stator resistance is identified online. Furthermore, when inductance reduces / increases to 80% / 120% of its initial value and permanent flux reduces to 80% / 70% of its initial value, the PMSM sensorless control has strong robustness to parameter perturbation.
- 3) The dynamic performance and tracking precision of the sensorless control and stator resistance identification could be improved when the DTCV scheme is employed.

In conclusion, using the proposed scheme, the performance of PMSM sensorless control is robust and effective. In future, experiments will be performed on industrial application scenario to further test the performance of the proposed control scheme.

REFERENCES

- [1] A. T. Woldegiorgis, X. Ge, H. Wang, and M. Hassan, "A new frequency adaptive second-order disturbance observer for sensorless vector control of interior permanent magnet synchronous motor," *IEEE Trans. Ind. Electron.*, vol. 68, no. 12, pp. 11847–11857, Dec. 2021.
- [2] W. He, X. Wu, J. Chen, and Y. Wang, "Comparative study of sensorless control of permanent magnet synchronous motor realised by sliding-mode observer," *IET Power Electron.*, vol. 13, no. 6, pp. 1191–1199, Feb. 2020.
- [3] C. Liu and J. Shang, "Sensorless drive strategy of open-end winding PMSM with zero-sequence current suppression," *IEEE Trans. Energy Convers.*, vol. 36, no. 4, pp. 2987–2997, Dec. 2021.
- [4] T. D. Do, H. H. Choi, and J. -W. Jung, "Nonlinear optimal DTC design and stability analysis for interior permanent magnet synchronous motor drives," *IEEE/ASME Trans. Mechatron.*, vol. 20, no. 6, pp. 2716–2725, Dec. 2015.
- [5] S. Murshid and B. Singh, "Implementation of PMSM drive for a solar water pumping system," *IEEE Trans Ind. Appl.*, vol. 55, no. 5, pp. 4956–4964, Sep./Oct. 2019.
- [6] A. V. R. Teja, V. Verma, and C. Chakraborty, "A new formulation of reactive-power-based model reference adaptive system for sensorless induction motor drive," *IEEE Trans. Ind. Electron.*, vol. 62, no. 11, pp. 6797–6808, Nov. 2015.
- [7] C. M. Verrelli *et al.*, "Speed sensor fault tolerant PMSM machines: From position-sensorless to sensorless control," *IEEE Trans. Ind. Appl.*, vol. 55, no. 4, pp. 3946–3954, Jul./Aug. 2019.
- [8] A. T. Woldegiorgis, X. Ge, S. Li, and M. Hassan, "Extended sliding mode disturbance observer-based sensorless control of IPMSM for medium and high-speed range considering railway application," *IEEE Access*, vol. 7, pp. 175302–175312, 2019.
- [9] X. Luo, A. Shen, Q. Tang, J. Liu, and J. Xu, "Two-step continuous-control set model predictive current control strategy for SPMSM sensorless drives," *IEEE Trans. Energy Convers.*, vol. 36, no. 2, pp. 1110–1120, Jun. 2021.
- [10] T. Wang, "An EMF observer for PMSM sensorless drives adaptive to stator resistance and rotor flux linkage," *IEEE J. Emerg. Sel. Topics Power Electron.*, vol. 7, no. 3, pp. 1899–1913, Sep. 2019.
- [11] J.-K. Seok, J.-K. Lee, and D.-C. Lee, "Sensorless speed control of nonsalient permanent-magnet synchronous motor using rotor-position-tracking PI controller," *IEEE Trans. Ind. Electron.*, vol. 53, no. 2, pp. 399–405, Apr. 2006.
- [12] T.-S. Low, T.-H. Lee, and K.-T. Chang, "A nonlinear speed observer for permanent-magnet synchronous motors," *IEEE Trans. Ind. Electron.*, vol. 40, no. 3, pp. 307–316, Jun. 1993.
- [13] F. Aghili, "Energy-efficient and fault-tolerant control of multiphase non-sinusoidal pm synchronous machines," *IEEE/ASME Trans. Mechatron.*, vol. 20, no. 6, pp. 2736–2751, Dec. 2015.
- [14] B. Stumberger, G. Stumberger, D. Dolinar, A. Hamler, and M. Trlep, "Evaluation of saturation and cross-magnetization effects in interior permanent-magnet synchronous motor," *IEEE Trans. Ind. Appl.*, vol. 39, no. 5, pp. 1264–1271, Sep. 2003.
- [15] Z. Yin, R. Tang, C. Du, and Y. Wang, "Moment of inertia identification based on unscented Kalman filter for permanent magnet synchronous motors," in *Proc. 14th IEEE Conf. Ind. Electron. Appl.*, Xi'an, China, 2019, pp. 1141–1145.
- [16] Y. Shi, K. Sun, L. Huang, and Y. Li, "Online identification of permanent magnet flux based on extended Kalman filter for IPMSM drive with position sensorless control," *IEEE Trans. Ind. Electron.*, vol. 59, no. 11, pp. 4169–4178, Nov. 2012.
- [17] A. Balamurali, C. Lai, G. Feng, V. Loukanov, and N. C. Kar, "Online multi-parameter identification of permanent magnet synchronous motors in EV application considering iron losses," in *Proc. XXII Int. Conf. Elect. Machines*, Lausanne, Switzerland, 2016, pp. 2306–2312.
- [18] S. J. Underwood and I. Husain, "Online parameter estimation and adaptive control of permanent-magnet synchronous machines," *IEEE Trans. Ind. Electron.*, vol. 57, no. 7, pp. 2435–2443, Jul. 2010.
- [19] G. V. Lakhekar, L. M. Waghmare, and R. G. Roy, "Disturbance observer-based fuzzy adapted S-surface controller for spatial trajectory tracking of autonomous underwater vehicle," *IEEE Trans. Intell. Veh.*, vol. 4, no. 4, pp. 622–636, Dec. 2019.
- [20] C. Zhou *et al.*, "An improved direct adaptive fuzzy controller of an uncertain PMSM for web-based e-service systems," *IEEE Trans. Fuzzy Syst.*, vol. 23, no. 1, pp. 58–71, Feb. 2015.
- [21] E. Zerdali and M. Barut, "MRAS based real-time speed-sensorless control of induction motor with optimized fuzzy-PI controller," in *Proc. IEEE Int. Symp. Sensorless Control Elect. Drives Predictive Control Elect. Drives Power Electron.*, Munich, Germany, 2013, pp. 1–5.
- [22] Y. Mei, K. Sun, and Y. Shi, "A 2-D fuzzy logic based MRAS scheme for sensorless control of interior permanent magnet synchronous motor drives with cyclic fluctuating loads," *Chin. J. Elect. Eng.*, vol. 1, no. 1, pp. 85–91, Dec. 2015.
- [23] S. E. Rezgui, S. Legrioui, A. Mehdi, and H. Benalla, "Robust IM control with MRAS-based speed and parameters estimation with ANN using exponential reaching law," in *Proc. Int. Conf. Control, Decis. Inf. Technol.*, Metz, France, 2014, pp. 477–482.
- [24] Z. -H. Liu, J. Nie, H. -L. Wei, L. Chen, X. -H. Li, and H. -Q. Zhang, "A newly designed VSC-based current regulator for sensorless control of PMSM considering VSI nonlinearity," *IEEE J. Emerg. Sel. Topics Power Electron.*, vol. 9, no. 4, pp. 4420–4431, Aug. 2021.
- [25] Y. A. I. Mohamed, "A newly designed instantaneous-torque control of direct-drive PMSM servo actuator with improved torque estimation and control characteristics," *IEEE Trans. Ind. Electron.*, vol. 54, no. 5, pp. 2864–2873, Oct. 2007.
- [26] K.-Y. Cheng and Y.-Y. Tzou, "Fuzzy optimization techniques applied to the design of a digital PMSM servo drive," *IEEE Trans. Power Electron.*, vol. 19, no. 4, pp. 1085–1099, Jul. 2004.
- [27] K. M. A. Prasad, U. Nair, and A. Unnikrishnan, "Fuzzy sliding mode control of a permanent magnet synchronous motor with two different fuzzy membership functions," in *Proc. Int. Conf. Power, Instrum., Control Comput.*, Thrissur, India, 2015, pp. 1–6.
- [28] M. N. Uddin, Z. R. Huang, and A. B. M. S. Hossain, "Development and implementation of a simplified self-tuned neuro-fuzzy-based IM drive," *IEEE Trans. Ind. Appl.*, vol. 50, no. 1, pp. 51–59, Jan./Feb. 2014.
- [29] F. Lin, I. Sun, K. Yang, and J. Chang, "Recurrent fuzzy neural cerebellar model articulation network fault-tolerant control of six-phase permanent magnet synchronous motor position servo drive," *IEEE Trans. Fuzzy Syst.*, vol. 24, no. 1, pp. 153–167, Feb. 2016.
- [30] Z.-H. Liu, H.-L. Wei, Q.-C. Zhong, K. Liu, and X.-H. Li, "GPU implementation of DPSSO-RE algorithm for parameters identification of surface PMSM considering VSI nonlinearity," *IEEE J. Emerg. Sel. Topics Power Electron.*, vol. 5, no. 3, pp. 1334–1345, Sep. 2017.
- [31] H.-S. Kim, H.-T. Moon, and M.-J. Youn, "On-line dead-time compensation method using disturbance observer," *IEEE Trans. Power Electron.*, vol. 18, no. 6, pp. 1336–1345, Nov. 2003.
- [32] G. Feng, C. Lai, K. Mukherjee, and N. C. Kar, "Current injection-based online parameter and VSI nonlinearity estimation for PMSM drives using current and voltage DC components," *IEEE Trans. Transport. Electrification.*, vol. 2, no. 2, pp. 119–128, Jun. 2016.

- [33] A. Mishra, G. Dubey, D. Joshi, P. Agarwal, and S. P. Sriavstava, "A complete fuzzy logic based real-time simulation of vector controlled PMSM drive," in *Proc. 2nd IEEE Int. Conf. Power Electron., Intell. Control Energy Syst.*, Delhi, India, 2018, pp. 809–814.
- [34] P. H. Krishnan and M. Arjun, "Control of BLDC motor based on adaptive fuzzy logic PID controller," in *Proc. Int. Conf. Green Comput. Commun. Elect. Eng.*, Coimbatore, India, 2014, pp. 1–5.
- [35] S. P. Singh, A. K. Gautam, J. Dubey, J. P. Pandey, and R. P. Payasi, "Performance comparison of PMSM drive using PI and fuzzy logic based controllers," in *Proc. IEEE Uttar Pradesh Sect. Int. Conf. Elect., Comput. Electron. Eng.*, Varanasi, India, 2016, pp. 563–569.
- [36] R. Na and X. Wang, "An improved vector-control system of PMSM based on fuzzy logic controller," in *Proc. Int. Symp. Comput., Consum. Control*, Taichung, Taiwan, 2014, pp. 326–331.
- [37] M. Tomita, T. Senjyu, S. Doki, and S. Okuma, "New sensorless control for brushless DC motors using disturbance observers and adaptive velocity estimations," *IEEE Trans. Ind. Electron.*, vol. 45, no. 2, pp. 274–282, Apr. 1998.



ZHAO-HUA LIU (Senior Member, IEEE) received the M.Sc. degree in computer science and engineering and the Ph.D. degree in automatic control and electrical engineering from the Hunan University, Changsha, China, in 2010 and 2012, respectively. From 2015 to 2016, he was a Visiting Researcher with the Department of Automatic Control and Systems Engineering, The University of Sheffield, Sheffield, U.K. He is currently a Professor of automatic control and systems with the School of Information and Electrical Engineering,

Hunan University of Science and Technology, Xiangtan, China. He has authored or coauthored more than 50 research papers in refereed journals and conferences, including IEEE TRANSACTIONS/Journal/Magazine. He is a regular reviewer for several international journals and conferences. His current research interests include intelligent information processing and control of wind turbines, computational intelligence and learning algorithms design, machine learning aided fault diagnosis and prognosis, parameter estimation and control of permanent-magnet synchronous machine drives, and fault diagnosis based intelligent operations and maintenance for electric power equipment.



JIE NIE received the B.Eng. degree in electrical engineering and automation in 2019 from the Hunan University of Science and Technology, Xiangtan, China, where he is currently working toward the M.S. degree in the electrical engineering.

His current research interests include parameter identification, and sensorless control for permanent magnet synchronous motor.



HUA-LIANG WEI received the Ph.D. degree in automatic control from The University of Sheffield, Sheffield, U.K., in 2004.

He is currently a Senior Lecturer with the Department of Automatic Control and Systems Engineering, The University of Sheffield, Sheffield, U.K. His research interests include evolutionary algorithms, identification and modelling for complex nonlinear systems, applications and developments of signal processing, system identification, and data modeling to control engineering.



LEI CHEN received the M.S. degree in computer science and engineering and the Ph.D. degree in automatic control and electrical engineering from the Hunan University, Changsha, China, in 2012 and 2017, respectively.

He is currently a Lecturer with the School of Information and Electrical Engineering, Hunan University of Science and Technology, Xiangtan, China. His current research interests include deep learning, network representation learning, information security of industrial control system, and Big

Data analysis.



XIAO-HUA LI received the B.Eng. degree in computer science and technology from the Hunan University of Science and Engineering, Yongzhou, China, in 2007, and the M.Sc. degree in computer science from Hunan University, Changsha, China, in 2010.

She is currently a Lecturer with the School of Information and Electrical Engineering, Hunan University of Science and Technology, Xiangtan, China. Her research focuses on evolutionary computation.



MING-YANG LV received the Ph.D. degree in control theory and engineering from Hunan University, Changsha, China, in 2020. He is currently a Lecturer with the School of Information and Electrical Engineering, Hunan University of Science and Technology, Xiangtan, China. His research interests include Chaos theory and application, modeling and fault diagnosis for complex system based on machine learning, and deep learning.